Mine Water and the Environment (2019) 38:643–657
https://doi.org/10.1007/s10230-019-00610-8

TECHNICAL ARTICLE

Water Conservation when Mining Multiple, Thick, Closely-Spaced Coal Seams: A Case Study of Mining Under Weishan Lake

Liqiang Ma[1,2] · Jinshuai Guo[3] · Wenpeng Liu[4] · Dongsheng Zhang[1] · Yihe Yu[1]

Received: 30 August 2018 / Accepted: 15 May 2019 / Published online: 23 May 2019

Abstract

To resolve issues of water resource conservation and avoid water inrush accidents, a case study was performed in the Gaozhuang coal mine, which lies under Weishan Lake. The two coal seams are 4 and 5 m thick, and are separated by 2–5 m. As the goaf gradually expanded with mining, some fractures that had formed at the centre of the goaf were gradually compressed and closed, while fractures at the periphery of the goaf did not. Therefore, the periphery of the goaf was recognized as the key region for water conservation mining. After the upper seam was mined, the hydraulically connected fractured (HCF) zone in the overburden had a maximum height of 6.9 times of the integrated mining height. After the lower seam was mined, the HCF zone increased to a maximum height of 9.8 times the integrated mining height. The maximum depth of ground surface fractures above the goaf was 1.1 times the integrated mining height. The thickness of the safety pillar to be left in place as protective strata was determined based on these values, and the hydraulic connection between the aquifers above the mine and the overlying lake was assessed. We then analysed the feasibility of in situ protection of the surface water and proposed techniques to prevent the water in the overlying sandstone from rushing into the work area.

Keywords Hydraulically conductive fracture (HCF) · Ground surface fracture (GSF) · Integrated mining height · Safety pillar · Water inrush

Introduction

Ecological problems, such as groundwater loss and drying up of springs and rivers, can result from coal mining. In China's Shendong mining area, for example, 19 of the 20 springs at the 131 km^2 Daliuta coal mine have already dried up (Fan et al. 2015). Therefore, minimizing the disturbance and damage to the local ecological environment through water conservation mining (WCM) is an urgent scientific problem in the further development of China's coal mines (Zhang et al. 2010). In addition to reducing the disturbance to the regional hydrological environment, WCM also aims to prevent water inrushes from coal mining to an allowable level by controlling the development of hydraulically conductive fractures (HCFs) into the mining-disturbed overburden. Fully understanding the characteristics of HCF development and distribution in such overburden is key to successful WCM (Adhikary and Guo 2014).

Relative to HCF development in overburden induced by mining of a single seam, Whittaker and Reddish (1989) divided the fractured region into continuous and

Electronic supplementary material The online version of this article (https://doi.org/10.1007/s10230-019-00610-8) contains supplementary material, which is available to authorized users.

✉ Liqiang Ma
ckma@cumt.edu.cn

✉ Jinshuai Guo
gjscumt@163.com

1 Key Laboratory of Deep Coal Resource Mining (CUMT), Ministry of Education, School of Mines, China University of Mining and Technology, Xuzhou 221116, China

2 College of Energy Engineering, Xi'an University of Science and Technology, Xi'an 710054, China

3 State Key Laboratory for Geomechanics and Deep Underground Engineering, School of Mechanics and Civil Engineering, China University of Mining and Technology, Xuzhou 221116, China

4 Department of Mining Engineering, Earth Mechanics Institute, Colorado School of Mines, Golden, CO 80401, USA

discontinuous fractured zones (Cherubini 2008; Moon and Jeong 2011; Whittaker and Reddish 1989). Forster and Enever (1992) suggested that the mining-disturbed overburden behind a longwall face can be split into four vertical zones: the caved, fractured, constrained, and surface zones. Kendorski subdivided the constrained zone into dilated and constrained zones, thus making a five-zone model (Galvin 2016; Kendorski 1993). Qian divided the mining-disturbed overburden into three zones: the caved, fractured, and subsidence zones (Qian and Miao 1995). Gao used a four-zone model, with a failure zone, separation zone, bending zone, and loose alluvium zone (Gao 1996). Moreover, based on borehole data from mining sites, Chinese researchers have derived empirical formulas for estimating the height of the HCF zone induced by coal mining in different geological conditions (Shi et al. 2012).

HCF development is different when mining coal seams that are near each other, due to the repeated disturbance of the overburden. Zhang and Hu found that the HCF zone's height in the overburden increased when continuously mining the lower seam due to the generation of new fractures and reactivation of existing fractures. Moreover, multiple factors, including the comprehensive thickness of the coal seams, distance between adjacent seams, and mining sequence, all affected the height of the HCF zone (Hu et al. 2015; Zhang 2010). Recent studies have revealed the pattern and development mechanism of HCF in overburden induced by mining shallowly buried coal seams that are near each other (Ma et al. 2015; Zhang et al. 2011a, b). In addition, these studies provided several approaches to control the HCF zone's height, such as arranging the faces in a staggered pattern, reducing the mining height, increasing the advance rate of the face, and using partial backfill mining.

Thus, researchers have mainly focused on variations in the height of the HCF. However, more studies are needed on the zoning characteristics of the HCF in different overlying strata and the redevelopment of this HCF due to repeated mining. We therefore studied the HCF induced by mining closely spaced thick seams under Weishan Lake and evaluated the feasibility of in situ lake water conservation. Furthermore, techniques for preventing water inrushes from the overlying sandstone were successfully applied to these coal seams.

Geological Conditions of the Study Area

Mining Geological Conditions

China has more than 25 billion metric tons (t) of coal reserves under water bodies, if one includes both surface water (lakes, reservoirs, and rivers) and aquifers in the overburden. The Weishan coal area is the largest mining area under a lake in China, with nearly 700 million t of coal reserves lying under the lake. Furthermore, Weishan Lake is situated in Shandong Province, in eastern China. It is a key nature reserve along the eastern route of the South-North Water Transfer Project. It is urgent in this area to minimize the impact of mining on local water resources while ensuring safety, namely to achieve WCM.

About two-thirds of the Gaozhuang coal mine in Jining City, its western portion, lies under Weishan Lake (Fig. 1). It has an annual production of 3.0 Mt, mining coal seams #31 and #32, which have average thicknesses of 5.0 and 4.0 m, respectively. The distance between seams #31 and #32 ranges from 2.0 to 7.0 m. This study focuses on working faces 31509 and 32509 in the no. 5 mining district, which is one of the six main districts in this mine (Fig. 2). Working face 31509 is 220 m wide and 1180 m long, and occurs at an average depth of 361 m, while working face 32509 is 189 m wide and 1270 m long, and has an average depth of 365 m. The inclined angle of the two working faces ranges from 0° to 5°, which has little effect on HCF development. Therefore, 0° was set as the inclined angle in this study for simplified calculation.

Hydrogeological Conditions

Figure 3 shows the stratigraphic column of the overburden above seams #31 and #32.

Aquifers

Aquifers can be classified into four types based on specific yield (Table 1). The main aquifers overlying the aforementioned seams include the upper Quaternary sandy mudstone (Aquifer 1), the lower Quaternary sandstone (Aquifer 2), the Jurassic sandy conglomerate (Aquifer 3), and the Permian sandstone (Aquifer 4).

1. Aquifer 1 has an average thickness of 39.5 m, with a specific yield of 0.2–3.4 L/s m and a permeability coefficient of 1.06×10^{-3}–4.94×10^{-6} m/d. It is classified as category II or III.
2. Aquifer 2 has an average thickness of 41 m, with a specific yield of 0.15–4.0 L/s m and a permeability coefficient of 1.16×10^{-3}–4.51×10^{-6} m/d. It is classified as category II or III.
3. Aquifer 3 has an average thickness of 103 m, with a specific yield of 0.04–0.5 L/s m and a permeability coefficient of 2.15×10^{-3}–3.04×10^{-6} m/d. It is classified as category III or IV.
4. Aquifer 4 has an average thickness of 77 m, with a specific yield of 7×10^{-5}–1.8×10^{-8} L/s m, and a permeability coefficient of 8.56×10^{-4}–1.05×10^{-6} m/d. It is classified as category IV.

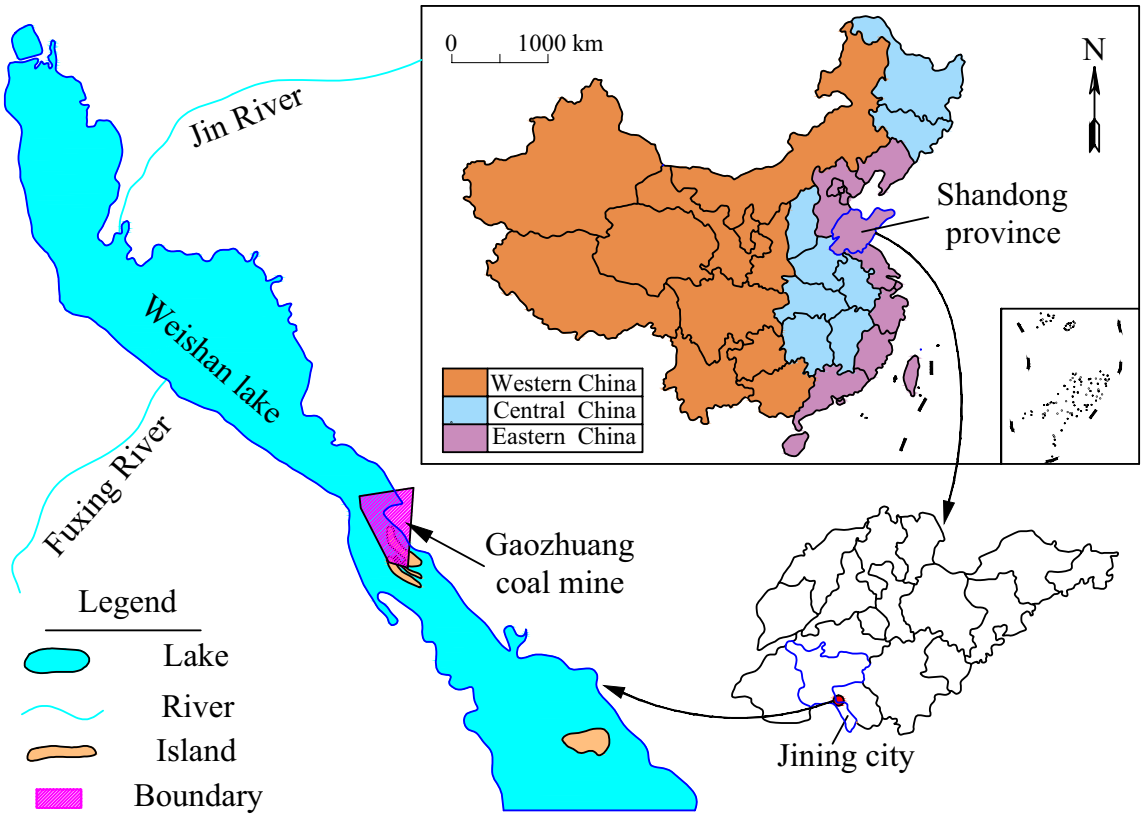

Fig. 1 Location of the coal mine

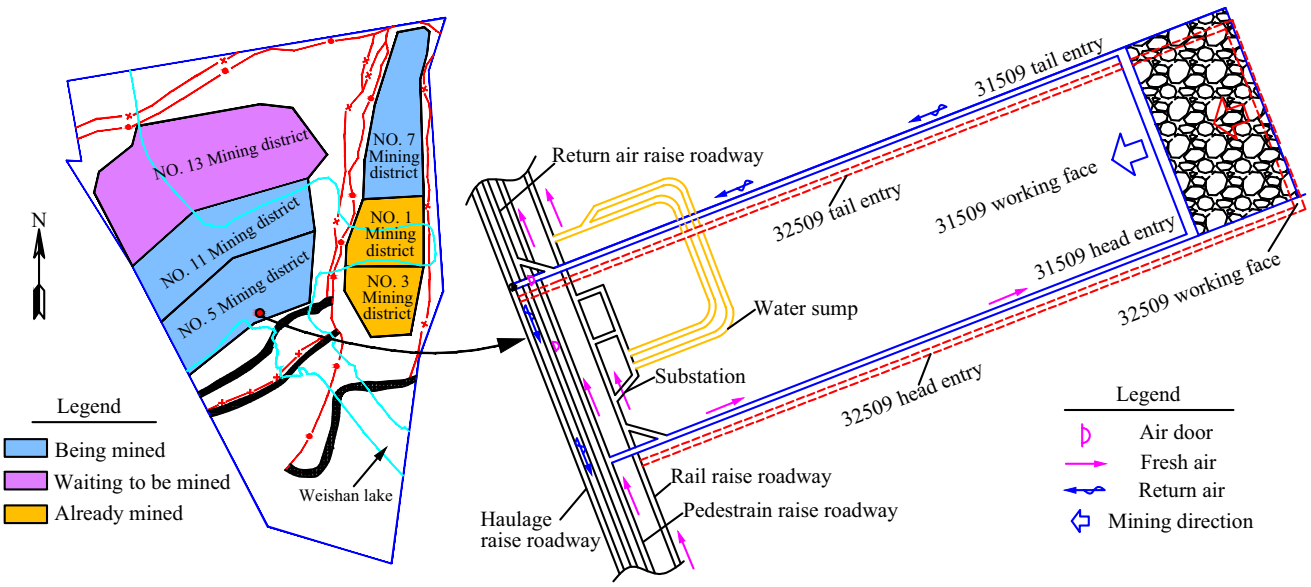

Fig. 2 Layout of the mining district and faces

Aquicludes

The overburden in the study area has three main aquicludes: the middle Quaternary clay (Aquiclude 1), siltstone at the bottom of the Quaternary (Aquiclude 2), and the mudstone and siltstone in the middle-upper part of the Permian (Aquiclude 3).

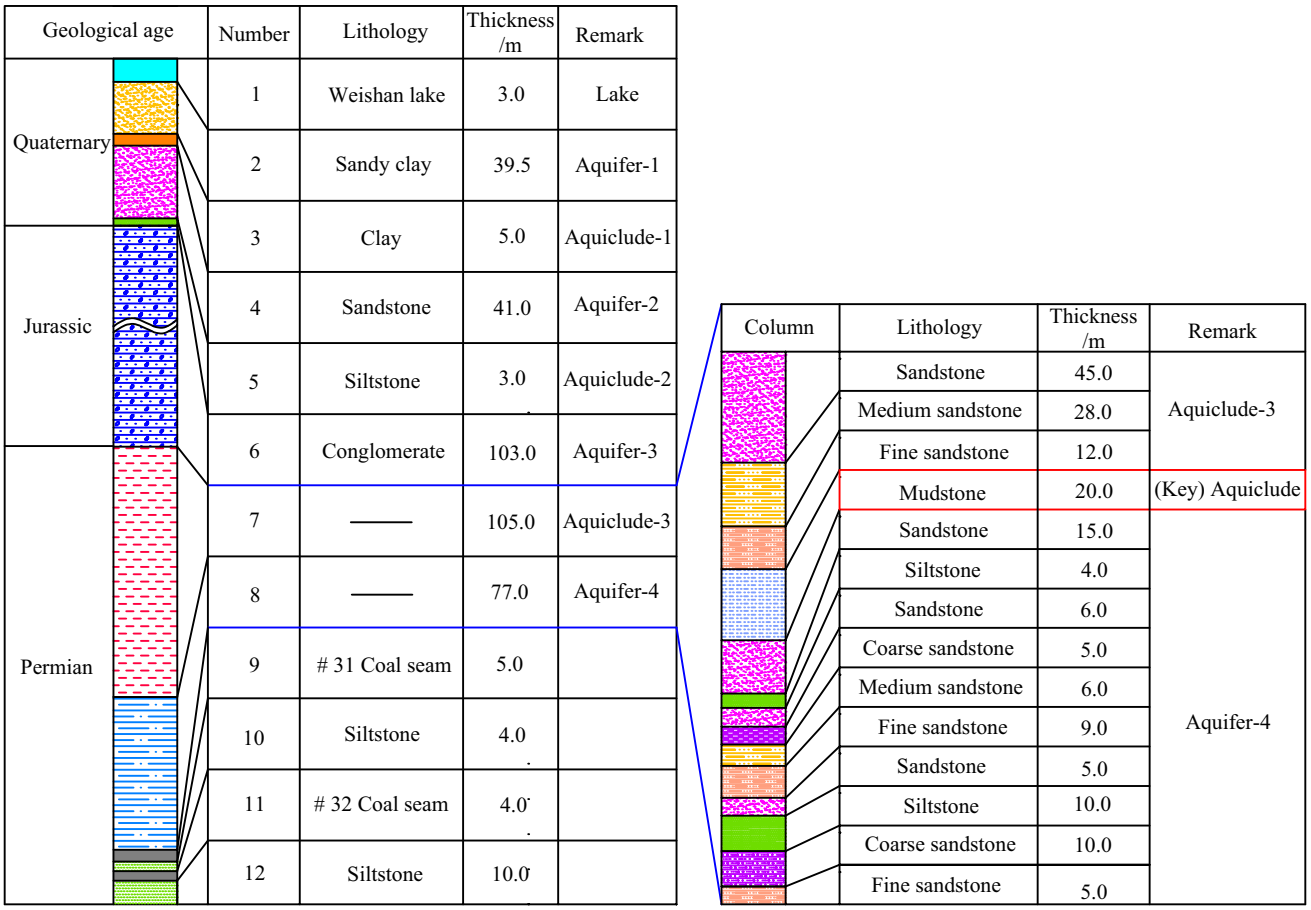

Fig. 3 Stratigraphic columns above seam #31 and #32

Table 1 Aquifer classification based on specific yield

Category	Type	Specific yield/L s^{-1} m^{-1}
I	Extreme high	≥5.0
II	High	1.0–5.0
III	Medium	0.1–1.0
IV	Low	≤0.1

1. Aquiclude 1 is composed of clay and sandy clay. Given its stability and high viscosity, this aquiclude effectively prevents surface water and groundwater in Aquifer 1 from passing through it.
2. Aquiclude 2 is tightly cemented, low-yielding, and impermeable to the groundwater in Aquifer 2.
3. Aquiclude 3, with an average thickness of 105 m, is characterized by low water yield and extremely low permeability. The 20 m thick mudstone is the key aquiclude that keeps the water in Aquifer 3 from percolating into the coal-bearing strata below.

Theoretical Calculations of HCF Zone's Height

Mining of the Single Seam

Based on long-term measurements from mine sites in central and eastern China, researchers have developed an empirical formula for calculating the height of the HCF zone (Sui et al. 2015):

$$H_{\mathrm{d}} = \frac{100\sum M}{K\sum M + a} \pm b \tag{1}$$

where M is the mining height (m); K, a, and b are pertinent parameters defined in terms of particular geological conditions.

The Gaozhuang coal mine has basically the same geological conditions as the nearby Cuizhuang, Jiangzhuang, and Fucun coal mines (Wang et al. 2016). An equation for predicting the maximum height of the HCF zone was derived

from the measured heights of HCF zones in the adjacent mines (Table 2) using linear regression analysis (Supplemental Fig. S-1).

$$H_{\mathrm{d}} = \frac{100\sum M}{0.4\sum M + 7.5} + 8.1 \tag{2}$$

Mining of Closely Overlying Seams

When the upper and lower coal seams are near each other, the corresponding caved and fractured zones induced by mining the upper and lower seams may partially overlap (Xu and Ju 2011). The scope of overlap depends on the distance between the two seams, h. When h is greater than the height of the lower caved zone, H_m, the lower caved zone will not overlap with the upper one. However, the two fractured zones may coincide. The heights of the upper and lower fractured zones can be estimated from the thicknesses of the upper and lower seams, separately. The larger value of the fractured zone's height is regarded as the comprehensive height of the fractured zone resulting from mining these two seams (Fig. 4a).

When $h < H_{\mathrm{m}}$, the maximum height of the upper fractured zone can be calculated from the thickness of the upper seam. The maximum height of the lower fractured zone can be derived from the integrated mining height of the two seams. The larger value can be used as the maximum height of the fractured zone induced by mining both seams (Fig. 4b). The integrated mining height for two seams is given by the equation below:

$$M_z = M_2 + \left(M_1 - \frac{h}{y_2}\right) \tag{3}$$

where M_z is the integrated mining height (m); M_1 is the thickness of the upper seam (m); M_2 is the thickness of the lower seam (m); h is the distance between the two seams (m); y_2 is the ratio of the lower caved zone's height to the mining height.

Table 2 Height of the HCF zone in adjacent coal mines

Number	Faces and coal mine	M/m	H_{d}/m
1	Face 31803 in Jangzhuang	4.3	54.6
2	Face 31706 in Jangzhuang	3.4	45.5
3	Face 31603 in Jangzhuang	3.8	47.5
4	Face 31903 in Jangzhuang	3.9	54.6
5	Face 3301 in Cuizhuang	5.0	59.5
6	Face 3302 in Cuizhuang	5.2	65.0
7	Face 3401 in Fucun	5.4	61.5
8	Face 3109 in Renchen	2.3	33.8
9	Face 32503 in Zhaoyang	2.0	33.2
10	Face 3202 Liangbaosi	3.0	43.0

In the study area, seam # 32 is 4.0 m thick, and the corresponding height of the caved zone is four times the mining height. The distance between seams #31 and #32 ranges from 2.0 to 7.0 m. So, the integrated mining height M_z is calculated at 8.6–8.9 m, and the maximum value (8.9 m) was used in this study. Separately substituting the mining height in seam #31 and the integrated mining height in seam #32 into Eq. 2 indicates that the maximum heights of the HCF zone at working faces 31509 and 32509 are 60.7 m and 88.6 m, respectively.

Numerical Simulation of Fracture Development in Overburden

The universal distinct element code (UDEC), a software program for discrete element modelling, is suitable for modelling the behaviour of discontinuous media (e.g. fractured or jointed rock masses) subjected to static or dynamic loading (Coggan et al. 2012; Ma et al. 2013). So, UDEC4.0 was used to simulate the fracture development in overburden disturbed by mining in the study area.

Model Parameters

A numerical model with the dimensions 300 m × 150 m was created to simulate the strata in the study area; separate 50 m thick boundaries were arranged on the left and right sides. Displacement constraints were applied to the

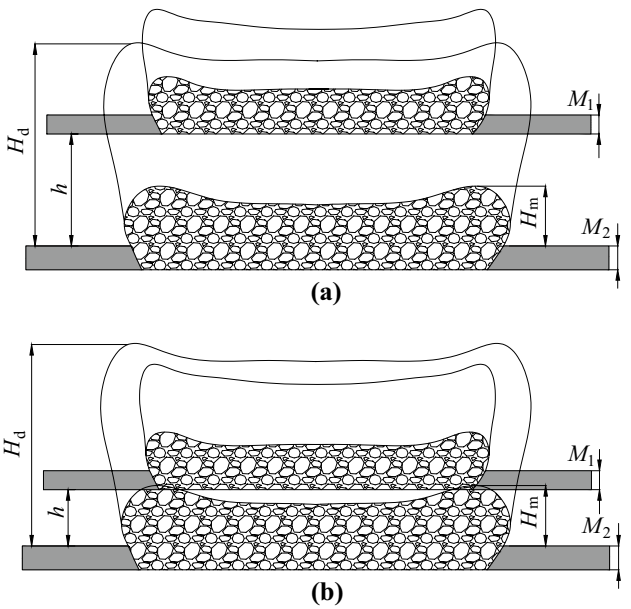

Fig. 4 Diagram of HCF zone's height induced by mining of close distance coal seams. $h > H_m$ (**a**); $h < H_m$ (**b**). (h is the distance between two seams, and H_m is the height of caved zone resulting from mining the lower seam.)

left, right, and bottom boundaries (Fig. 5). The 127 m strata immediately above seam #31 were modelled, while the rest of the overburden was represented as pressure exerted on the top of the model. The Mohr–Coulomb failure criterion was applicable to the model (Yang et al. 2016). Parameters of the blocks and joints in the model are shown in Supplemental Tables S-1 and S-2.

In the simulation, working face 31509 in the upper seam was mined first, followed by working face 32509 in the lower seam. The coal was mined in multiple stages, and the working face advanced 20 m in each stage, which is equal to the periodic weighting interval. The total advanced distance of each working face was 200 m (the face had reached the stage of critical mining where the maximum subsidence value in the surface would not grow as the face advances). Monitoring lines were laid out in the overburden above face 31509 to collect stress and displacement data during mining. Their distances from face 31509 were 5 m (the immediate roof), 15 m (the main roof), 25 m, 39 m, 50 m, 60 m, 75 m (the key aquiclude), and 95 m, respectively.

Analysis of Numerical Simulation Results

The distribution of fractures in the model was visualized by UDEC (Majdi et al. 2012; Maximovich and Khayrulina 2014). Mining-induced fractures in the overburden are shown in the red region in Figs. 6 and 7.

Fracture Development Induced by Mining the Upper Seam

Figure 6 reveals that as working face 31509 advanced 40 m, vertical fractures developed in the overburden above the open-off cut and the mining side, and horizontal fractures developed above the working face. The fracture height reached up to 17 m. As the working face advanced 80 m, fractures over the two sides, or periphery, of the goaf continued growing upward. Moreover, fractures generated above the middle of the working face developed to the bottom of sandstone, with a height of up to 60 m.

As the goaf expanded, fractures over the middle of the goaf partially closed due to compression, and the fracture height was reduced to 56 m. In comparison, fractures on the sides of the working face were unlikely to close (Palchik 2010); however, the maximum development height, about 62 m, did not reach the key aquiclude.

Fracture Development Induced by Mining of the Lower Seam

As working face 32509 advanced, the closed fractures over the central section of the upper goaf were reactivated and continued to develop (Fig. 7). After mining stopped, fractures over the central part of the goaf reached a height of 76 m; the maximum fracture height, 86 m, occurred in the peripheral zone.

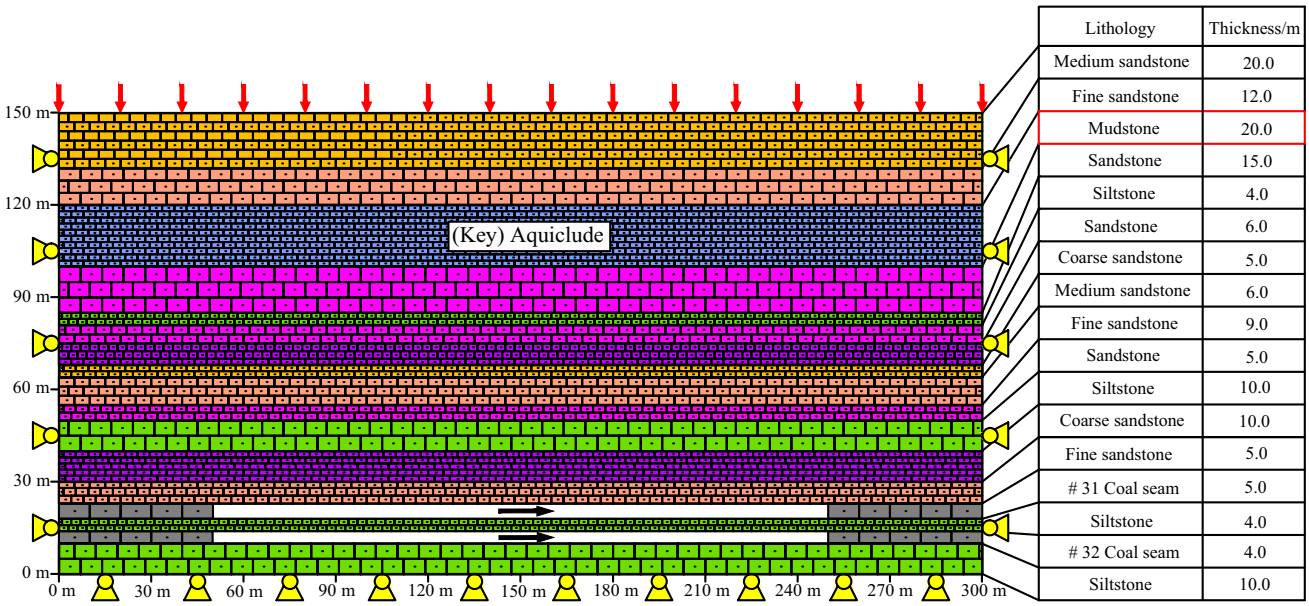

Lithology	Thickness/m
Medium sandstone	20.0
Fine sandstone	12.0
Mudstone	20.0
Sandstone	15.0
Siltstone	4.0
Sandstone	6.0
Coarse sandstone	5.0
Medium sandstone	6.0
Fine sandstone	9.0
Sandstone	5.0
Siltstone	10.0
Coarse sandstone	10.0
Fine sandstone	5.0
# 31 Coal seam	5.0
Siltstone	4.0
# 32 Coal seam	4.0
Siltstone	10.0

Fig. 5 Numerical simulation model

Zoning Characteristics of Overburden Based on Fractures

Figure 8 illustrates the distribution of fractures in the overburden after completion of mining at working faces 31509 and 32509. Based on the level of fracture development, the overburden can be partitioned into four zones: the interconnected fracture zone, fracture development zone, micro-fracture zone, and unfractured zone (Zuo et al. 2018). The fracture development and micro-fracture zones constitute the HCF. The height of the HCF above the central section of the goaf was about 10.6% less than the peripheral HCF. Therefore, the overburden above the periphery of the goaf is the key region for WCM.

Supplemental Fig. S-2 shows the distribution of ground subsidence caused by mining working face 31509. The overburden along the central section of the goaf had subsided uniformly, while the overburden along two sides experienced non-uniform subsidence. Fractures within the zone of the uniform subsidence were likely to be closed due to compression, while in the zones of non-uniform subsidence, fractures tended to develop due to the tension (Guo et al. 2017; Yang et al. 2015).

Field Observations of the HCF Zone

Underground Drilling and Water Injection Observation

Observation Principles

The height of the HCF zone in mining-disturbed overburden can be observed by a variety of methods, including ultrasound imaging, computed tomography (CT) of boreholes, transient electromagnetics, hydrological observation through surface drilling, and underground drilling and water injection (UDWI). Ultrasound imaging, CT of boreholes, and transient electromagnetics are usually used as supplementary methods because of their strict requirements, complex operations, and large errors. Hydrological observation through surface drilling normally involves massive amounts of work, long duration, and high costs, and is easily affected by topography and surface architectures. The UDWI method is applicable to all mining sites, is cost-effective, and allows reliable, continuous monitoring (Luan et al. 2010; Majdi et al. 2012).

UDWI was employed in this study. In this method, boreholes are drilled into the roof above the main roadways that serve two working faces. A double-headed plug is inserted into each borehole to create an interval within a certain stratum, and water is then injected into the interval. Afterward, the amount of water that leaks from this stratum is measured. Then the position of the plug is changed and the injection and measurements are repeated to monitor the water leakage from different strata. The height of the HCF zone in the overburden can be determined by comparing the amounts of water leakage before and after mining (Supplemental Fig. S-3).

Observation Procedures

Figure 9 shows the schematic of the equipment used in the observation. Fig. S-4 illustrates the observational procedures. The procedures are detailed as follows (Zhang et al. 2015; Zhao et al. 2015):

Step 1: open the air injection system so that the capsules will expand and block/seal both ends of the borehole.
Step 2: open the water injection system to inject water into the borehole at a water pressure less than the capsule pressure.
Step 3: when the water injection and the leakage from the fractures in the wall become stable, use a flow meter to measure the injection rate; in other words, the rate of water leakage from the wall.
Step 4: after the test is completed, close the water injection valve and open the drain valve to drainater out of the sealed borehole interval.
Step 5: change plug positions and repeat the previous steps. In this way, the leakage from consecutive intervals of a borehole are obtained. The measured water leakage can be used as a criterion to assess the level of fracture development and therefore to determine the height of HCF zone.

Layout of Observation Site

The numerical simulation revealed that the height of the HCF zone above the periphery of the goaf was greater than in other overburden areas. Therefore, the field observation mainly focused on sites in the periphery of the goaf. One pre-mining observation borehole and two post-mining observation boreholes were drilled in each roadway. The pre-mining borehole was used to observe the pre-existing fractures in the undisturbed overburden, while the post-mining boreholes were used to monitor fractures in the mining-disturbed overburden. The height of the HCF zone in the overburden was then determined by comparing data collected from the pre-mining and post-mining observations (Gao et al. 2014; Xu et al. 2012).

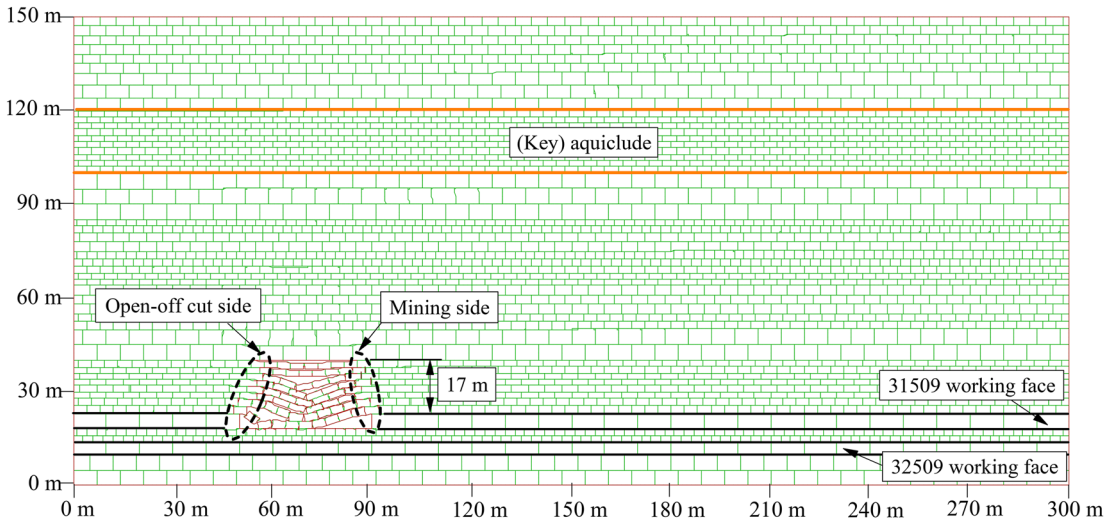
150 m
120 m
90 m
60 m
30 m
0 m
(Key) aquiclude
Open-off cut side
Mining side
17 m
31509 working face
32509 working face
0 m
30 m
60 m
90 m
120 m
150 m
180 m
210 m
240 m
270 m
300 m

(a)

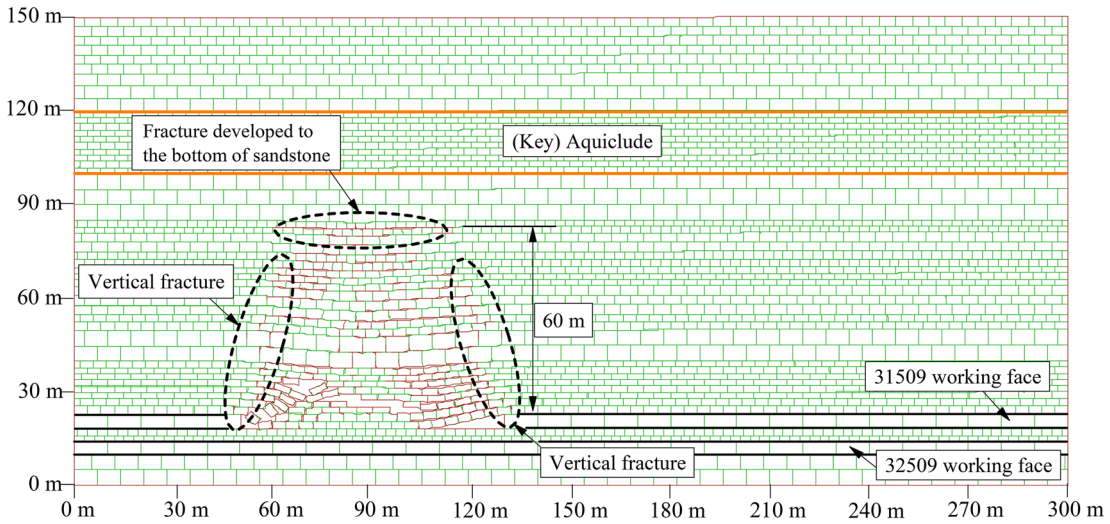
150 m
120 m
90 m
60 m
30 m
0 m
Fracture developed to the bottom of sandstone
(Key) Aquiclude
Vertical fracture
60 m
31509 working face
Vertical fracture
32509 working face
0 m
30 m
60 m
90 m
120 m
150 m
180 m
210 m
240 m
270 m
300 m

(b)

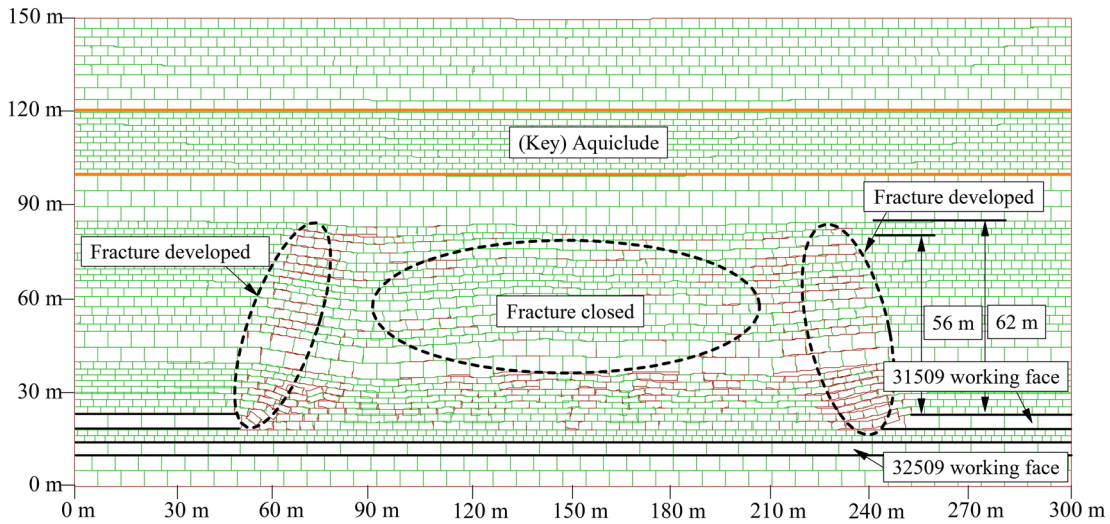
150 m
120 m
90 m
60 m
30 m
0 m
(Key) Aquiclude
Fracture developed
Fracture developed
Fracture closed
56 m
62 m
31509 working face
32509 working face
0 m
30 m
60 m
90 m
120 m
150 m
180 m
210 m
240 m
270 m
300 m

(c)

◂**Fig. 6** Fracture development induced by mining of working face 31509. Working face 31509 advanced 40 m (**a**); Working face 31509 advanced 80 m (**b**); Working face 31509 advanced 200 m (**c**)

Borehole Locations

As boreholes should be placed where the overburden will be sufficiently disturbed by mining, the drill sites were located near where mining stopped (Wang et al. 2008). Post-mining observational boreholes were drilled in the 4th to 5th month after extraction was completed, 30 m in front of where mining stopped in each seam (Fig. 10).

Borehole Inclination

To reduce drilling length and engineering cost, increase effective flushing of the boreholes while drilling, and ensure effective of plugging to create a sealed borehole interval, the borehole inclination should be as great as possible. The observation boreholes in working face 31509 were designed with an inclined angle of 45°. Given that the working faces 32509 and 31509 were arranged in a staggered pattern, observation boreholes for working face 32509 were drilled into the upper goaf at an inclination of 60° to avoid the other boreholes.

Borehole Length

The length of the boreholes has to exceed the estimated maximum height of the HCF zone and should sufficiently extend into the rock mass. Thus, the effects of the borehole inclination should be accounted for to define the borehole length (Fig. 10). The borehole length for working faces 31509 and 32509 were determined as 90 and 120 m, respectively. Other boreholes parameters are given in Table 3.

$$H_d = L \sin \beta \tag{4}$$

where H_d is the height of HCF zone; L is the borehole length; and β is the borehole's inclined angle.

Observation Approach

In each borehole, observations started at a shallow point and then gradually proceeded deeper. To improve efficiency, the observations were performed primarily at the middle and deep areas of the borehole (Luan et al. 2012). Based on the theoretical results and field experience, the initial observation points at faces 31509 and 32509 were located at positions with vertical depths of 25 and 55 m, respectively.

Observation Results

HCF Zone's Height After Mining of the Upper Seam

1. Fig. 11 shows that the leakage in borehole $1^{\#}$ remained at 20 L/min. This is because the overburden was undisturbed, and the water injected into the borehole primarily flowed in the pre-existing fractures.
2. Many new fractures developed in the overburden that was disturbed by mining. The initial leakage flow in boreholes $2^{\#}$ and $3^{\#}$ peaked at 34 L/min, about 70% greater than in borehole $1^{\#}$ at the same depth (in the fracture development zone). As the observation depth increased, the leakage from boreholes $2^{\#}$ and $3^{\#}$ decreased significantly, which indicated that the corresponding borehole intervals were in the micro-fracture zone. In the last interval, the volume of leakage flow in these two boreholes was fairly stable and about equal to the level of borehole $1^{\#}$. This interval corresponded to the unfractured zone.
3. As shown in Fig. 11a, b, the leakage curves for boreholes $1^{\#}$ and $2^{\#}$ intersect at a depth of 58.6 m, while the leakage curves for boreholes $1^{\#}$ and $3^{\#}$ intersect at 62.9 m. The results from the two post-mining observation boreholes reveals that the height of the HCF zone at face 31509 was 60.8 m.

The HCF Zone's Height After Mining of the Lower Seam

1. The initial leakage volume in borehole $6^{\#}$ basically stayed stable at 40 L/min, which was twice the initial leakage volume in boreholes $2^{\#}$ and $3^{\#}$ (Fig. 12). This is primarily because the closed fractures in the overburden were reactivated after working face 32509 was mined.
2. The leakage curves for boreholes $4^{\#}$ and $5^{\#}$ intersect at a vertical depth of 85.1 m (Fig. 12b), and those for boreholes $4^{\#}$ and $6^{\#}$ meet at a vertical depth of 88.5 m. The results from the two post-mining observation boreholes suggests that the height of HCF zone at face 32509 was 86.8 m.

Depth of the Ground Surface Fracture (GSF) Induced by Mining

The overburden movement caused by coal mining can create a subsidence trough over the goaf, and fractures develop in the periphery of the subsidence trough due to tensile deformation (Fig. 13). Stress–strain analysis of the element at a fracture tip indicates that the critical point for fracture development satisfies the following condition (Wang et al. 2013).

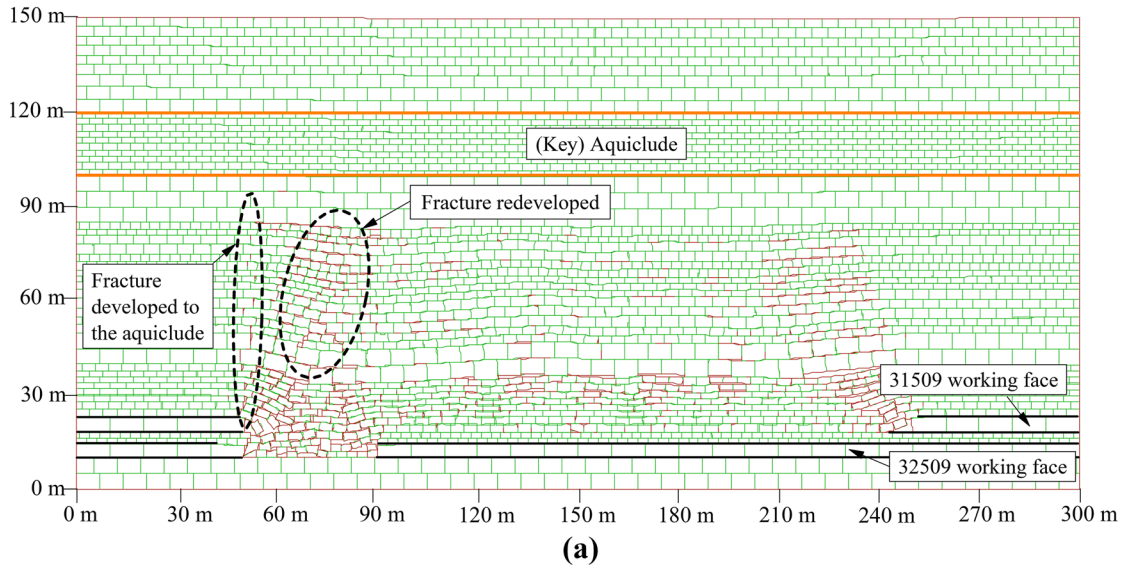
150 m
120 m
90 m
60 m
30 m
0 m
(Key) Aquiclude
Fracture redeveloped
Fracture developed to the aquiclude
31509 working face
32509 working face
0 m
30 m
60 m
90 m
120 m
150 m
180 m
210 m
240 m
270 m
300 m

(a)

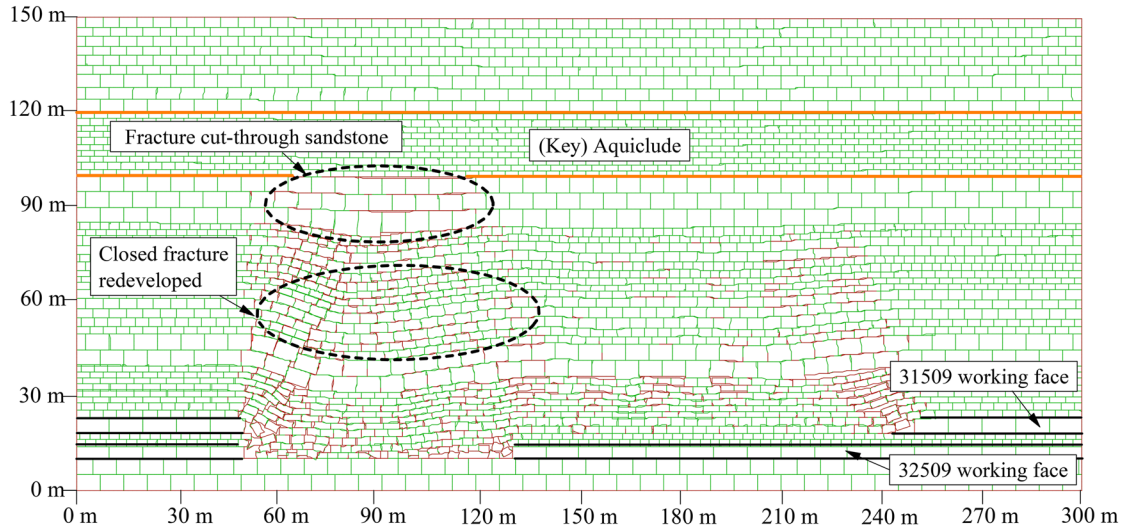
150 m
120 m
90 m
60 m
30 m
0 m
Fracture cut-through sandstone
(Key) Aquiclude
Closed fracture redeveloped
31509 working face
32509 working face
0 m
30 m
60 m
90 m
120 m
150 m
180 m
210 m
240 m
270 m
300 m

(b)

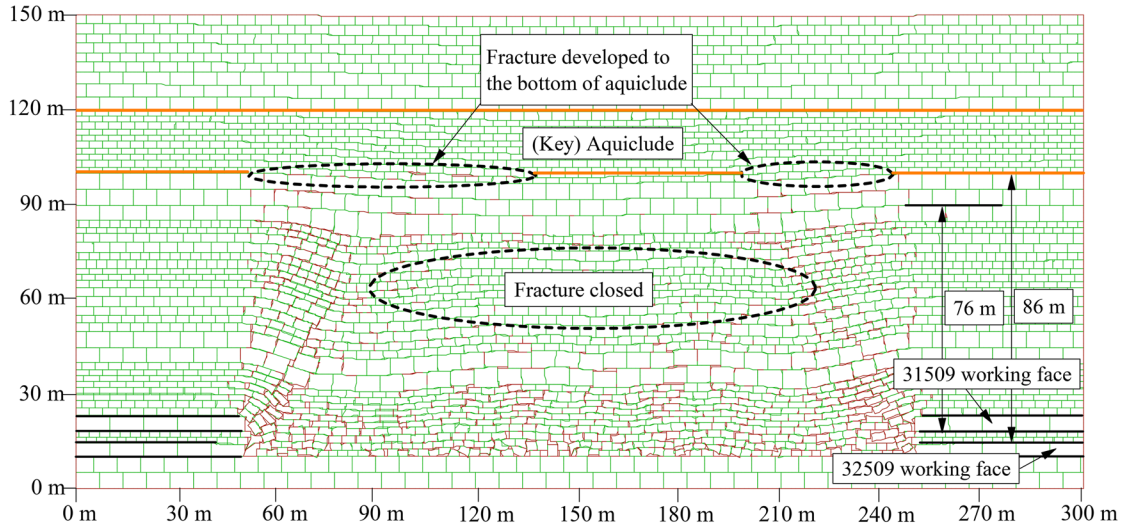
150 m
120 m
90 m
60 m
30 m
0 m
Fracture developed to the bottom of aquiclude
(Key) Aquiclude
Fracture closed
76 m
86 m
31509 working face
32509 working face
0 m
30 m
60 m
90 m
120 m
150 m
180 m
210 m
240 m
270 m
300 m

(c)

◂**Fig. 7** Fracture development induced by mining of working face 32509. Working face 32509 advanced 40 m (**a**); Working face 32509 advanced 100 m (**b**); Working face 32509 advanced 200 m (**c**)

$$\begin{cases} \varepsilon_h + \varepsilon_v \geq 0 \\ \varepsilon_h < \varepsilon_l \end{cases} \tag{5}$$

where ε_h is horizontal deformation, which tends to decrease with increasing depth in the surface tensile zone; ε_v is vertical deformation, which tends to increase with increasing depth in the surface tensile zone; and ε_l is the critical horizontal deformation of surface strata.

According to the plane strain condition in the theory of elasticity, we have

$$\begin{cases} \varepsilon_h = \frac{1-v^2}{E}\left(\sigma_h - \frac{v}{1-v}\sigma_v\right) \\ \varepsilon_v = \frac{1-v^2}{E}\left(\sigma_v - \frac{v}{1-v}\sigma_h\right) \end{cases} \tag{6}$$

Let $\sigma_h = -\gamma h$ (only the strata weight is considered), $\varepsilon_v = \varepsilon_h$, and $\varepsilon_h = \varepsilon_l$, and substitute these into Eq. 6. Given that the GSF would be partially closed after intrusion of lake water, a healing coefficient $\alpha = 0.8$, was introduced.

$$h = \frac{\alpha}{\gamma}\frac{E\varepsilon_l}{(1+v)(2v+1)} \tag{7}$$

Assuming that GSFs terminate at positions where $\sigma_1 = \sigma_h$ and $\sigma_3 = \sigma_v = 0$, and substituting these into the limit state condition in the Mohr–Coulomb theory yields the following equation:

$$\varepsilon_l = \frac{2C(1-v^2)\tan(45° + 0.5\varphi)}{E} \tag{8}$$

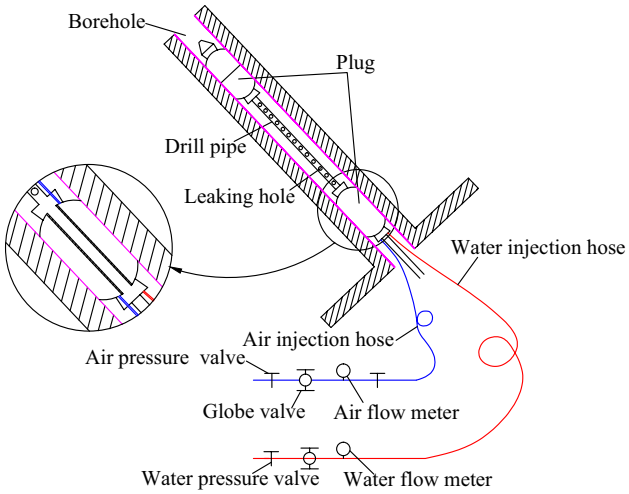

Fig. 9 Schematic of the equipment for UDWI

where C is cohesion and φ is the angle of internal friction. The rock mechanics parameters of the upper sandstone over faces 31509 and 32509 involve $E = 10$ GPa, $v = 0.25$, $C = 5$ MPa, and $\varphi = 30$ (the parameter values may be smaller in common sandstone due to long-term exposure to lake water). The deformation was calculated at $\varepsilon_l = 1.85$ mm. Substituting the deformation into Eq. 7, the depth of GSF above the goaf was 9.5 m.

Field Application

Given the location of Weishan Lake, in situ lake water conservation can be achieved by leaving a sufficiently thick safety pillar. Techniques such as advanced drilling drainage

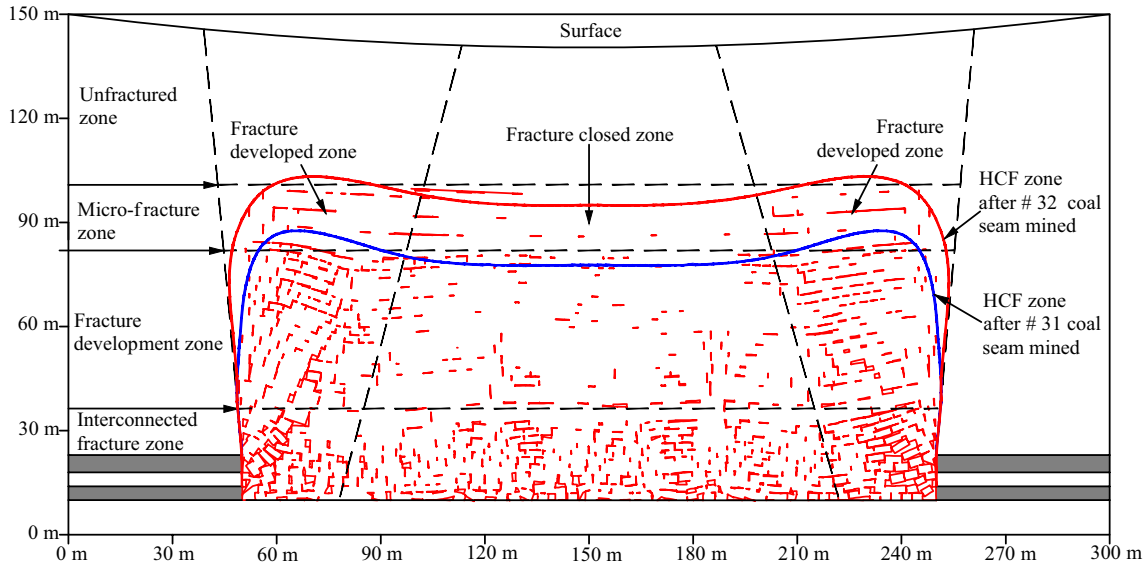

Fig. 8 Zones characteristics in the overburden

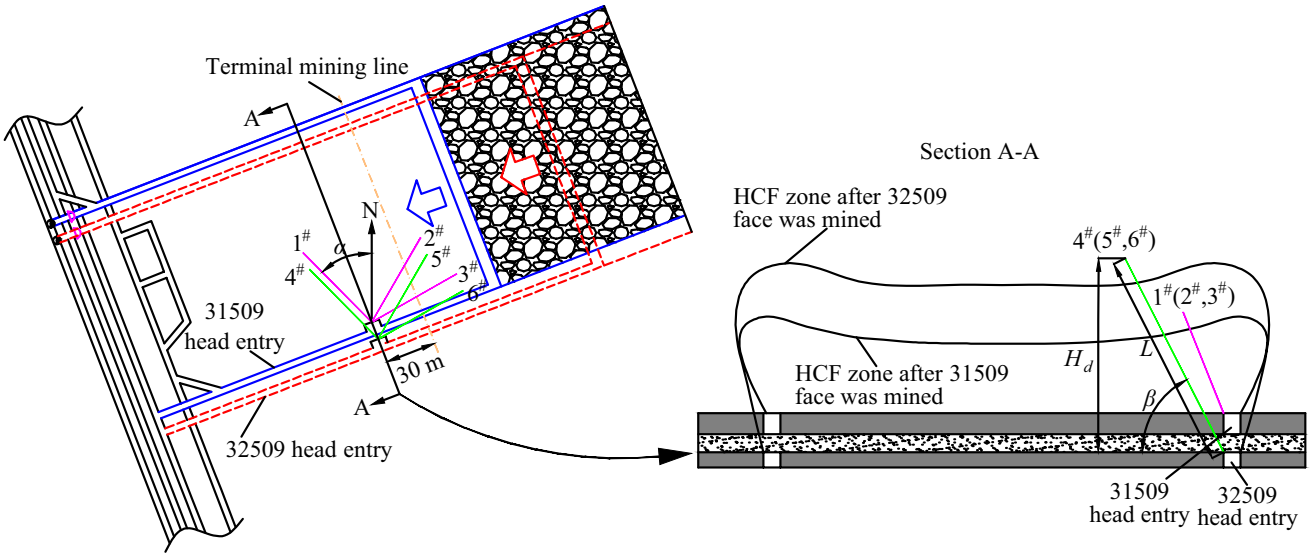

Fig. 10 Schematic plan and profile of the drill site

Table 3 Parameters of boreholes

Face	Borehole	Type	Diameter/mm	Azimuth angle/°	Inclined angle/°	Length/m	H_d/m
31509	1#	Pre-mining	75	315°	70°	90	85
	2#	Post-mining	75	30°	70°	90	85
	3#	Post-mining	75	60°	70°	90	85
32509	4#	Pre-mining	75	315°	60°	120	104
	5#	Post-mining	75	30°	60°	120	104
	6#	Post-mining	75	60°	60°	120	104

can be used to prevent accidents as long as the water-bearing sandstone in the roof has no hydraulic connection with the lake water (Howladar 2013; Maximovich and Khayrulina 2014). Therefore, based on previous analysis on the height of HCF zone and the depth of the GSF, we determined the proper thickness of the safety pillar to effectively prevent a hydraulic connection between the sandstone and lake water. In addition, using other secondary techniques to reinforce the sandstone roof strata, the objective of performing water conservation mining in coal seams under the Weishan Lake was ultimately achieved.

In-Situ Lake Water Conservation

Height of the HCF Zone

The maximum height of the HCF zone was used as its ultimate height. The height of the HCF zone induced by mining at working face 31509 was 6.9 times of the integrated mining height, while it was 9.8 times the integrated mining height for working face 32509 (Table 4).

Feasibility of In-Situ Conservation

After working faces 31509 and 32509 were mined, the maximum depth of the GSF was about 1.1 times the integrated mining height, while the maximum height of the HCF zone in the overburden was 9.8 times the integrated mining height. The distance from the upper boundary of the HCF zone to the lake floor was 32.2 times the integrated mining height, which meets the requirement that the thickness of an underwater safety pillar should be at least 7 times the mining height. This should guarantee that a hydraulic connection will not form between the water in the sandstone roof strata and lake water, and that in situ lake water conservation is achieved.

Prevention of Water Inrushes from the Roof Sandstone Strata

Given that the HCF in the overburden induced by mining faces 31509 and 32509 had extended to Aquifer 4, advanced

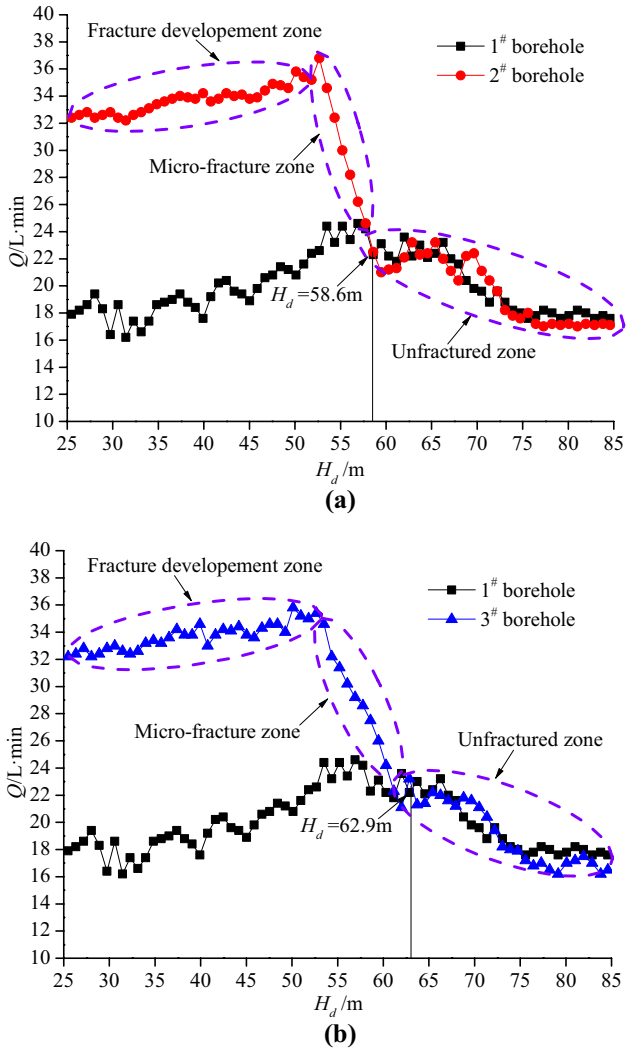

Fig. 11 Observation data of boreholes in face 31509. Observation data of borehole 1# and 2# (**a**); Observation data of borehole 1# and 3# (**b**)

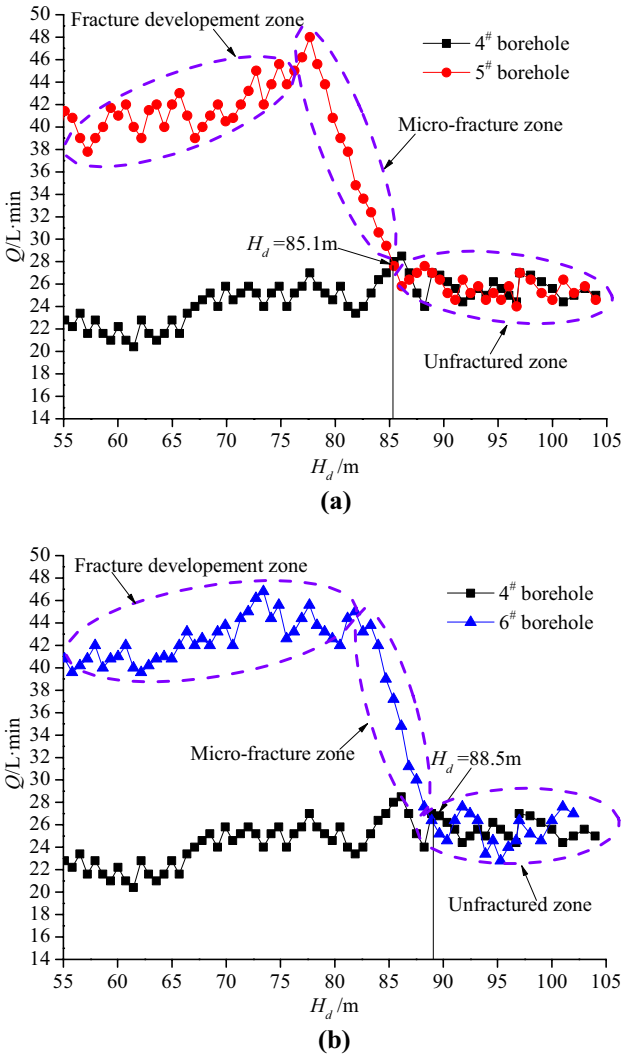

Fig. 12 Observation data of boreholes in face 32509. Observation data of borehole 4# and 5# (**a**); Observation data of borehole 4# and 6# (**b**)

drilling drainage and grouting were needed to ensure safe mining (Zhang et al. 2011a, b).

Drainage boreholes were drilled into the roof 200 m ahead of the working face above the main roadways along each face. Then, water was drained from Aquifer 4 thorough the boreholes to mitigate the risk of inrushes.

Since geological structures in the surrounding rock could be hydraulically connected to other water bodies, grouting was also implemented. Since grout normally spreads over a radius of 2.0–3.0 m, the grouting borehole spacing was set at 5.0 m.

After these measures were implemented, the water inflow at working face 31509 decreased from 100 m^3/h to 20 m^3/h, and from 120 m^3/h to 40 m^3/h at working face 32509. Eventually, both working faces were mined out safely without any water inrush accidents.

Conclusions

1. The overburden can be divided based on the level of fracture development induced by mining, from bottom to top: the interconnected fracture zone, the fracture development zone, the micro-fracture zone, and the unfractured zone. The fracture development and micro-fracture zones constitute the HCF zone. As the working face advanced, fractures over the central part of the goaf were partially closed by compression. The peripheral fractures were difficult to close and their heights were 10.6% greater than those above the central area. This indicates that the overburden over the periphery of the goaf is the key region for WCM.

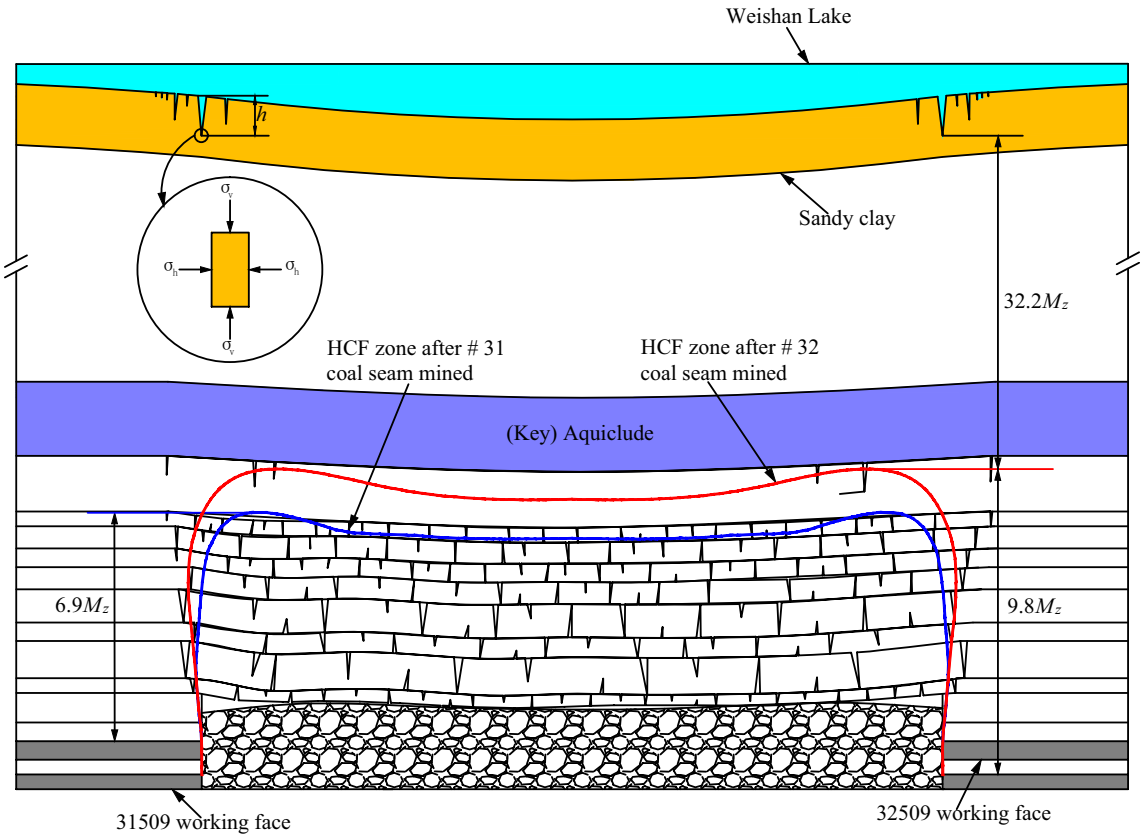

Fig. 13 Schematic of fractures in the overburden induced by mining

Table 4 Height of HCF zone

Face	Theoretical calculation/m	Numerical simulation/m	Field observation/m	Average/m	H_d/M_z
31509	60.7	62.0	60.8	61.2	6.9
32509	88.6	86.0	86.8	87.1	9.8

2. After the upper seam was mined, the HCF zone had a maximum height 6.9 times the integrated mining height. When the lower seam was mined, the closed fractures became reactivated and continued to grow. The maximum height of the HCF zone grew to 9.8 times the integrated mining height, about a 42% increase. The GSF developed in the lake bottom sediment would partially close after intrusion of the lake water. The maximum depth of GSF was 1.1 times the integrated mining height.
3. After the two neighboring coal seams were mined, the distance from the upper boundary of the HCF zone to the Weishan Lake bottom was 32.2 times the integrated mining height. This distance is enough to prevent a hydraulic connection between the water contained in the roof sandstone strata and the lake water. However, considering that the HCF in the overburden extended to the water-bearing Permian sandstone, advanced drainage and local grouting techniques were carried out to prevent a water inrush accident. With these measures, the objective of WCM under Weishan Lake was achieved.
4. The characteristics of fracture development in closely adjacent, thick coal seams were determined. These can be used for WCM and to prevent water inrush events under all kinds of water bodies.

Acknowledgements This work was supported by the Fundamental Research Funds for the Central Universities (2017XKQY096) and the Priority Academic Program Development of Jiangsu Higher Education Institutions.

References

Adhikary DP, Guo H (2014) Measurement of longwall mining induced strata permeability. Geotech Geol Eng 32(3):617–626

Cherubini CA (2008) modeling approach for the study of contamination in a fractured aquifer. Geotech Geol Eng 26(5):519–533
Coggan J, Gao F, Stead D, Elmo D (2012) Numerical modelling of the effects of weak immediate roof lithology on coal mine roadway stability. Int J Coal Geol 90–91(1):100–109
Fan LM, Ma XD, Ji RJ (2015) Progress in engineering practice of water-preserved coal mining in western eco-environment frangible area. J Chin Coal Soc 40(8):1711–1717 **(in Chinese)**
Forster IR, Enever J (1992) Hydrogeological response of overburden to underground mining. Off Energy Rep 1:104
Galvin JM (2016) Ground engineering-principles and practices for underground coal mining. Springer, Switzerland
Gao YF (1996) Rock shift "four band" model and dynamic displacement back analysis. J Chin Coal Soc 1:51–56 **(in Chinese)**
Gao BB, Liu YP, Pan JY, Yuan T (2014) Detection and analysis of height of water flowing fractured zone in underwater mining. Chin J Rock Mech Eng s1:3384–3390 **(in Chinese)**
Guo JS, Ma LQ, Wang Y, Wang FT (2017) Hanging wall pressure relief mechanism of horizontal section top-coal caving face and its application—a case study of the Urumqi coalfield, China. Energies 10(9):1371
Howladar FM (2013) Coal mining impacts on water environs around the Barapukuria coal mining area, Dinajpur, Bangladesh. Environ Earth Sci 70(1):215–226
Hu YZ, Liu CQ, Liu CY, Xhen BB (2015) Development regularity of mining-induced fractures in mixed mining of coal seam group. J Min Saf Eng 32(3):396–400 **(in Chinese)**
Kendorski FS (1993) Some modes of deformation and failure of lined tunnels. Int J Rock Mech Min 30(7):1497–1501
Luan YC, Li JT, Ban XH, Shang CY, Zhang CQ, Ma DP (2010) Observational research on the height of water flowing fractured zone in repeated mining of short-distance coal seams. J Min Saf Eng 27(1):143–146 **(in Chinese)**
Luan YC, Li JT, Liu N, Liu Y, Luan HX, Ma DP (2012) Research on overlying strata and surface movement rule in repeated mining. J Min Saf Eng 29(1):90–94 **(in Chinese)**
Ma LQ, Cao XQ, Liu Q, Zhou T (2013) Simulation study on water-preserved mining in multi-excavation disturbed zone in close-distance seams. Environ Eng Manag J 12(9):1849–1853
Ma LQ, Jin ZY, Liang JM, Sun H, Zhang DS, Li P (2015) Simulation of water resource loss in short-distance coal seams disturbed by repeated mining. Environ Earth Sci 74(7):5653–5662
Majdi A, Hassani FP, Nasiri MY (2012) Prediction of the height of destressed zone above the mined panel roof in longwall coal mining. Int J Coal Geol 98(1):62–72
Maximovich N, Khayrulina E (2014) Artificial geochemical barriers for environmental improvement in a coal basin region. Environ Earth Sci 72(6):1915–1924
Moon J, Jeong S (2011) Effect of highly pervious geological features on ground-water flow into a tunnel. Eng Geol 117(3):207–216 **(in Chinese)**
Palchik V (2010) Experimental investigation of apertures of mining-induced horizontal fractures. Int J Rock Mech Min 47(3):502–508
Qian MG, Miao XX (1995) Theoretiacal analysis on the structukal form and stability of overlying strata in longwall mining. Chin J Rock Mech Eng 14(2):97–106 **(in Chinese)**
Shi LQ, Xin HQ, Zhai PH, Li SC, Liu TB, Yan Y, Wei WX (2012) Calculating the height of water flowing fracture zone in deep mining. J Chin Univ Min Technol 41(1):37–41 **(in Chinese)**
Sui WH, Hang Y, Ma LX, Wu ZY, Zhou YJ, Long GQ, Wei LB (2015) Interactions of overburden failure zones due to multiple-seam mining using longwall caving. Bull Eng Geol Environ 74(3):1019–1035
Wang ZX, Zhang WQ, Zhao DS (2008) Continuous exploration for deformation and failure of overburdens under injecting grouts in separate layers. Chin J Geol Eng 30(7):1094–1098 **(in Chinese)**
Wang ZX, Zhao DS, Xia HC, Fan C (2013) The hazard geo-analysis of water inrush of mining of thick coal seam under reservoir. J Chin Coal Soc 38(a02):370–376 **(in Chinese)**
Wang FT, Tu SH, Zhang C, Zhang YW, Bai QS (2016) Evolution mechanism of water-flowing zones and control technology for longwall mining in shallow coal seams beneath gully topography. Environ Earth Sci 75(19):1309
Whittaker BN, Reddish DJ (1989) Subsidence occurrence, prediction and control. Elsevier, Amsterdam
Xu JL, Ju JF (2011) Structural morphology of key stratum and its influence on strata behaviors in fully-mechanized face with super-large mining height. Chin J Rock Mech Eng 30(8):1547–1556 **(in Chinese)**
Xu JL, Zhu WB, Wang XZ (2012) New method to predict the height of fractured water-conducting zone by location of key strata. J Chin Coal Soc 37(5):762–769 **(in Chinese)**
Yang YG, Wang J, Yu YJ (2015) Effects of different coal safe mining sequence under river on height of water flowing fracture zone. J Chin Coal Soc 40(s1):27–32 **(in Chinese)**
Yang SQ, Chen M, Jing HW, Chen KF, Meng B (2016) A case study on large deformation failure mechanism of deep soft rock roadway in Xin'An coal mine, China. Eng Geol 217:89–101
Zhang YJ (2010) Research on failure height and characteristic of overlying strata in mining coal seams with small interval. Coal Min Technol 15(6):9–11 **(in Chinese)**
Zhang DS, Fan GW, Liu YD, Ma LQ (2010) Field trials of aquifer protection in longwall mining of shallow coal seams in China. Int J Rock Mech Min 47(6):908–914
Zhang DS, Fan GW, Ma LQ, Wang XF (2011a) Aquifer protection during longwall mining of shallow coal seams: a case study in the Shendong Coalfield of China. Int J Coal Geol 86(2):190–196
Zhang QC, Li JH, Liu BS, Chen XJ (2011b) Directional drainage grouting technology of coal mine water damage treatment. Proc Eng 26:264–270
Zhang Y, Zhang CL, Zhao P (2015) Dynamic evolution rules of mining-induced fractures in different floor area of short-distance coal seams. J Min Saf Eng 40(4):786–792 **(in Chinese)**
Zhao BC, Liu ZR, Tong C, Wang CL (2015) Relation between height of water flowing fractured zone and mining parameters. J Min Saf Eng 32(4):634–638 **(in Chinese)**
Zuo JP, Sun YJ, Wang JT, Shi Y, Wen JT (2018) Mechanical and numerical analysis of "analogous hyperbola" movement of overlying strata after full mining extraction. J Min Saf Eng 1:71–77 **(in Chinese)**